Title
Electron scattering by magnetosonic waves in the inner magnetosphere

Journal
Journal of Geophysical Research Space Physics, 121(1)

ISSN
2169-9380

Authors
Ma, Qianli
Li, Wen
Thorne, Richard M
et al.

Publication Date
2016

DOI
10.1002/2015ja021992

Peer reviewed

AGU PUBLICATIONS

JGR

Journal of Geophysical Research: Space Physics

RESEARCH ARTICLE
10.1002/2015JA021992

Key Points:
- A new statistics of magnetosonic waves is performed
- Magnetosonic waves can lead to the butterfly distributions of energetic electrons
- Typical acceleration of electrons by magnetosonic waves is slower than energization by chorus

Correspondence to:
Q. Ma,
qianlima@atmos.ucla.edu

Citation:
Ma, Q., W. Li, R. M. Thorne, J. Bortnik, C. A. Kletzing, W. S. Kurth, and G. B. Hospodarsky (2016), Electron scattering by magnetosonic waves in the inner magnetosphere, *J. Geophys. Res. Space Physics*, *121*, 274–285, doi:10.1002/2015JA021992.

Received 4 OCT 2015
Accepted 21 DEC 2015
Accepted article online 28 DEC 2015
Published online 20 JAN 2016

Electron scattering by magnetosonic waves in the inner magnetosphere

Qianli Ma[1], Wen Li[1], Richard M. Thorne[1], Jacob Bortnik[1], C. A. Kletzing[2], W. S. Kurth[2], and G. B. Hospodarsky[2]

[1]Department of Atmospheric and Oceanic Sciences, University of California, Los Angeles, California, USA, [2]Department of Physics and Astronomy, University of Iowa, Iowa City, Iowa, USA

Abstract We investigate the importance of electron scattering by magnetosonic waves in the Earth's inner magnetosphere. A statistical survey of the magnetosonic wave amplitude and wave frequency spectrum, as a function of geomagnetic activity, is performed using the Van Allen Probes wave measurements and is found to be generally consistent with the wave distribution obtained from previous spacecraft missions. Outside the plasmapause the statistical frequency distribution of magnetosonic waves follows the variation of the lower hybrid resonance frequency, but this trend is not observed inside the plasmasphere. Drift and bounce averaged electron diffusion rates due to magnetosonic waves are calculated using a recently developed analytical formula. The resulting timescale of electron energization during disturbed conditions (when $AE^* > 300$ nT) is more than 10 days. We perform a 2-D simulation of the electron phase space density evolution due to magnetosonic wave scattering during disturbed conditions. Outside the plasmapause, the waves accelerate electrons with pitch angles between 50° and 70° and form butterfly pitch angle distributions at energies from ~100 keV to a few MeV over a timescale of several days; whereas inside the plasmapause, the electron acceleration is very weak. Our study suggests that intense magnetosonic waves may cause the butterfly distribution of radiation belt electrons especially outside the plasmapause, but electron acceleration due to magnetosonic waves is generally not as effective as chorus wave acceleration.

1. Introduction

Fast magnetosonic waves are highly oblique whistler-mode electromagnetic emissions generated in the frequency range between the local proton gyrofrequency (f_{cp}) and the lower hybrid resonance frequency (f_{LHR}) [e.g., *Perraut et al*., 1982; *Laakso et al*., 1990; *Santolík et al*., 2002] and are primarily observed by spacecraft within 5° of the Earth's magnetic equator [*Russell and Holzer*, 1970; *Němec et al*., 2005, 2006; *Pokhotelov et al*., 2008; *Santolík et al*., 2004]. The waves occur over a broad spatial region between 2 R_E and 8 R_E both inside and outside the plasmapause, with highest wave intensities observed near the dayside during geomagnetically disturbed conditions [*Meredith et al*., 2008; *Ma et al*., 2013; *Němec et al*., 2015]. Ion ring distributions provide free energy for the local excitation of magnetosonic waves when the ion ring energy is close to the local Alfven energy and typically occur over a broad region outside the plasmapause and near the outer edge of the plasmasphere [*Chen et al*., 2010; *Jordanova et al*., 2012; *Ma et al*., 2014a]. The injected ion populations may account for the excitation of magnetosonic waves especially on the dayside outside the plasmapause [*Boardsen et al*., 1992; *Chen et al*., 2011; *Thomsen et al*., 2011; *Xiao et al*., 2013], and the excited waves then propagate in both radial and azimuthal directions [e.g., *Xiao et al*., 2012]. Magnetosonic waves propagate nearly perpendicularly to the background magnetic field near the equatorial plane [*Kasahara et al*., 1994; *Chen and Thorne*, 2012], and the waves inside the plasmapause may become naturally trapped within the plasmasphere [*Ma et al*., 2014b].

The energetic electron populations in the Earth's outer radiation belt can experience diffusive scattering by various plasma waves [*Kennel and Engelmann*, 1966; *Lyons*, 1974a, 1974b]. Two important magnetospheric waves that cause local electron acceleration in the radiation belts are whistler-mode chorus and magnetosonic waves [*Thorne*, 2010]. The Van Allen Probes observations and their related simulation studies have confirmed that whistler-mode chorus waves provide sufficient local heating of energetic electrons in the heart of radiation belts during geomagnetic storm periods [*Reeves et al*., 2013; *Thorne et al*., 2013; *Foster et al*., 2014; *Li et al*., 2014b]. On the other hand, intense magnetosonic wave events are observed by the spacecraft in the inner magnetosphere and could have a potential role in electron acceleration via Landau resonance and transit-time scattering effects [*Horne et al*., 2007; *Bortnik and Thorne*, 2010; *Li et al*., 2014a]. During Landau resonant

interactions, the electrons experience a nearly constant parallel electric field in the moving frame. Interactions with the magnetosonic wave mainly cause the acceleration of electrons in the parallel direction with respect to the background magnetic field. *Bortnik and Thorne* [2010] also found that electrons typically experience only a fraction of the magnetosonic wavelength during their bounce motion across the equatorial plane. The wave electric fields perpendicular to the background magnetic field in the frame of the moving electrons cause additional scattering due to a transit-time effect. Both quasi-linear theory calculations [*Horne et al*., 2007] and test-particle simulations [*Bortnik and Thorne*, 2010; *Li et al*., 2014a] indicate that the timescale of electron acceleration due to an intense magnetosonic wave event with an amplitude of ~ 218 pT observed by Cluster is about 1 day. However, the relative role of equatorial magnetosonic waves (compared to chorus) in electron scattering is an important unresolved question in the Earth's radiation belt dynamics.

A detailed evaluation of electron scattering due to typical magnetosonic waves at different locations and under different conditions is required to determine whether magnetosonic waves need to be included in radiation belt simulations. The Van Allen Probes have nearly equatorial orbits and provide an excellent opportunity to compile statistics of the magnetosonic wave amplitude distribution and the wave frequency spectrum. *Mourenas et al*. [2013] have provided analytical formulae to calculate the Landau scattering of electrons due to magnetosonic waves without the inclusion of transit-time scattering and evaluated the potential importance of magnetosonic waves on electron energization compared with chorus waves and on the pitch angle scattering compared with plasmaspheric hiss. *Bortnik et al*. [2015] have developed analytical formulae to calculate the electron diffusion coefficients due to equatorial magnetosonic wave scattering, providing an efficient tool to accurately estimate both Landau resonance and transit-time effects. The analytical formulae have been proven to capture most of the wave scattering features predicted by test-particle simulations. The statistical wave distribution and the analytical formulae of diffusion coefficients can be used to estimate the global wave scattering rates and obtain an understanding of the averaged effects of magnetosonic waves under typical conditions.

This paper is organized as the following: in section 2, we present the global distributions of equatorial magnetosonic wave amplitudes and wave frequency spectra using recent Van Allen probes observations; the electron scattering effects due to typical magnetosonic waves are analyzed in section 3; and we summarize our results and discuss the potential roles of magnetosonic waves in section 4.

2. Van Allen Probes Statistics of Magnetosonic Waves

The Van Allen Probes were launched into near-equatorial orbits with a perigee of ~ 1.1 R_E and an apogee of ~ 5.9 R_E on 30 August 2012 [*Mauk et al*., 2012]. The twin probes (Probe A and B) are equipped with high-resolution wave and particle instruments and provide excellent plasma wave measurements in the inner magnetosphere. The magnetometer and the Waves instrument of the Electric and Magnetic Field Instrument Suite and Integrated Science (EMFISIS) [*Kletzing et al*., 2013] provide measurements of the background magnetic field and the wave electric and magnetic fields, respectively. The waveform receiver (WFR) of the Waves instrument measures wave power spectral density from about 10 Hz to 12 kHz for all three components of both electric and magnetic fields. The WFR also provides wave polarization properties including wave normal angle and ellipticity, calculated using the Singular Value Decomposition method [*Santolík et al*., 2003]. The high-frequency receiver (HFR) of the Waves instrument measures the electric field spectral density from 10 kHz to 400 kHz [*Kletzing et al*., 2013], which covers most of the upper hybrid resonance frequency (f_{UHR}) range in the inner magnetosphere and can be used to infer the total electron density and identify the plasmapause location [*Kurth et al*., 2015].

Figure 1 presents a magnetosonic wave event observed by Van Allen Probe A on 6 October 2012. The *AE* index (Figure 1a) briefly increased to ~400 nT at around 0120 UT, then diminished for 8 h and then increased again and remained high (between 300 and 600 nT) from 1000 UT to 1700 UT. Electrostatic electron cyclotron harmonic (ECH) waves are clearly observed at frequencies between f_{ce} (the solid white line) and f_{UHR} outside the plasmapause (Figure 1b). The intensity of ECH waves can be used to identify whether the spacecraft is in the plasmasphere or in the plasmatrough region [e.g., *Meredith et al*., 2004]. The plasmapause indicator (pp) is shown in Figure 1c with 1 denoting that the spacecraft is outside the plasmapause and 0 denoting that it is inside the plasmapause. Equatorial magnetosonic waves are observed between the proton gyrofrequency f_{cp} (long-dashed black line in Figure 1d) and the lower hybrid resonance frequency f_{LHR} (solid black line in

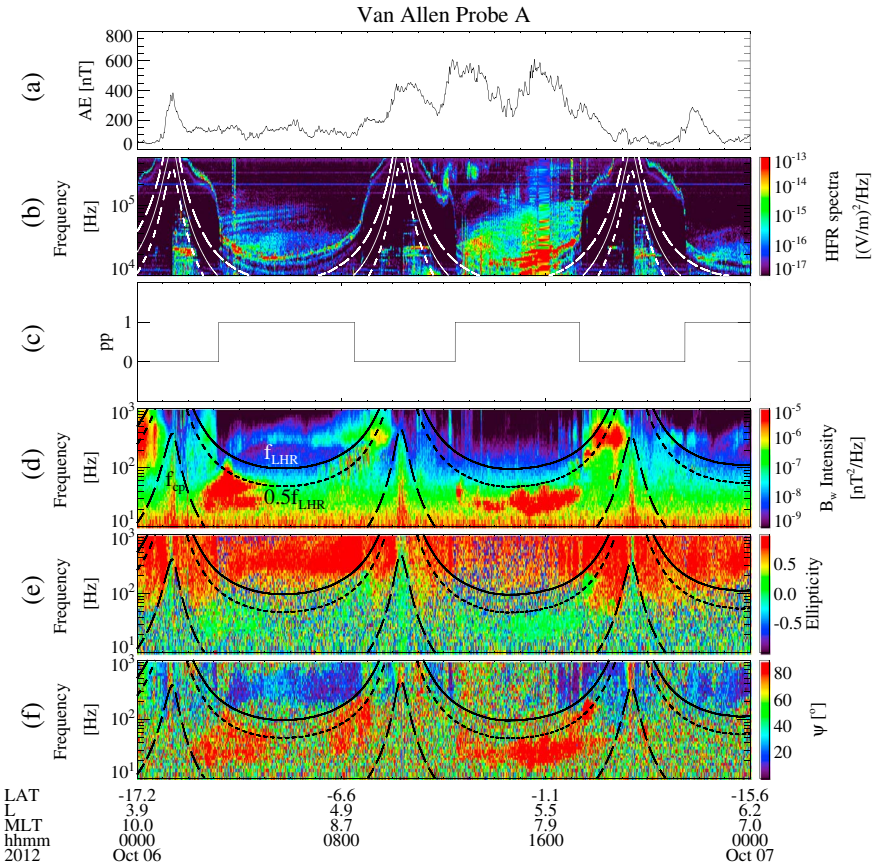

Figure 1. Magnetosonic waves observed by Van Allen Probe A on 6 October 2012. (a) The *AE* index, (b) electric field power spectral density in the Waves HFR channel, (c) plasmapause indicator inferred from ECH wave intensities (1: outside; 0: inside), (d) magnetic field power spectral density in the Waves WFR channel, (e) wave ellipticity, and (f) wave normal angle. The white long-dashed, solid, and dashed lines in Figure 1b represent the frequencies of 2 f_{ce}, f_{ce}, and 0.5 f_{ce}, respectively; the black solid, dashed, and long-dashed lines in Figures 1d–1f represent the frequencies of f_{LHR}, 0.5 f_{LHR}, and f_{cp}, respectively.

Figure 1d). In Figure 1d, magnetosonic waves with magnetic intensities higher than 10^{-6} nT^2/Hz are observed between 20 and 150 Hz from 0230 UT to 0500 UT, between 20 and 60 Hz from 1230 UT to 1730 UT, and between 120 Hz and 220 Hz from 1730 UT to 1800 UT. Magnetosonic waves are identified as the highly oblique, nearly linearly polarized electromagnetic emissions. To clearly identify magnetosonic wave activity, we require the absolute value of the wave ellipticity (Figure 1e) to be lower than 0.2, and the wave normal angle (Figure 1f) to be higher than 80°. Using these criteria, the magnetosonic waves are automatically selected among other plasma waves that may coexist in the same frequency band (e.g., hiss emissions) in the wave power spectrogram. The magnetosonic wave amplitude is obtained by integrating over the selected magnetosonic wave magnetic power intensities.

We have surveyed the magnetosonic wave intensities from 20 Hz to 4 kHz using the Van Allen Probes WFR data set from October 2012 to April 2015. Figure 2 presents the global distribution of root-mean-square (RMS) averaged magnetosonic wave amplitudes between 2 R_E and 6 R_E, categorized by different *AE** conditions, latitudinal ranges, and whether the waves are observed inside or outside the plasmapause. Here *AE** is the maximum *AE* value in the preceding 3 h. The sample numbers (N_s) on each right bottom global dial show that the 31 month survey provides sufficient data coverage to obtain good wave statistics. The white area represents the bins with N_s less than 100 counts, which we subsequently exclude from our analysis.

The magnetosonic wave amplitude survey by the Van Allen Probes is qualitatively consistent with the previous Time History of Events and Macroscale Interactions during Substorms (THEMIS) statistics obtained during a relatively quiet period between 2010 and 2012 [*Ma et al.*, 2013] and the previous Cluster statistics

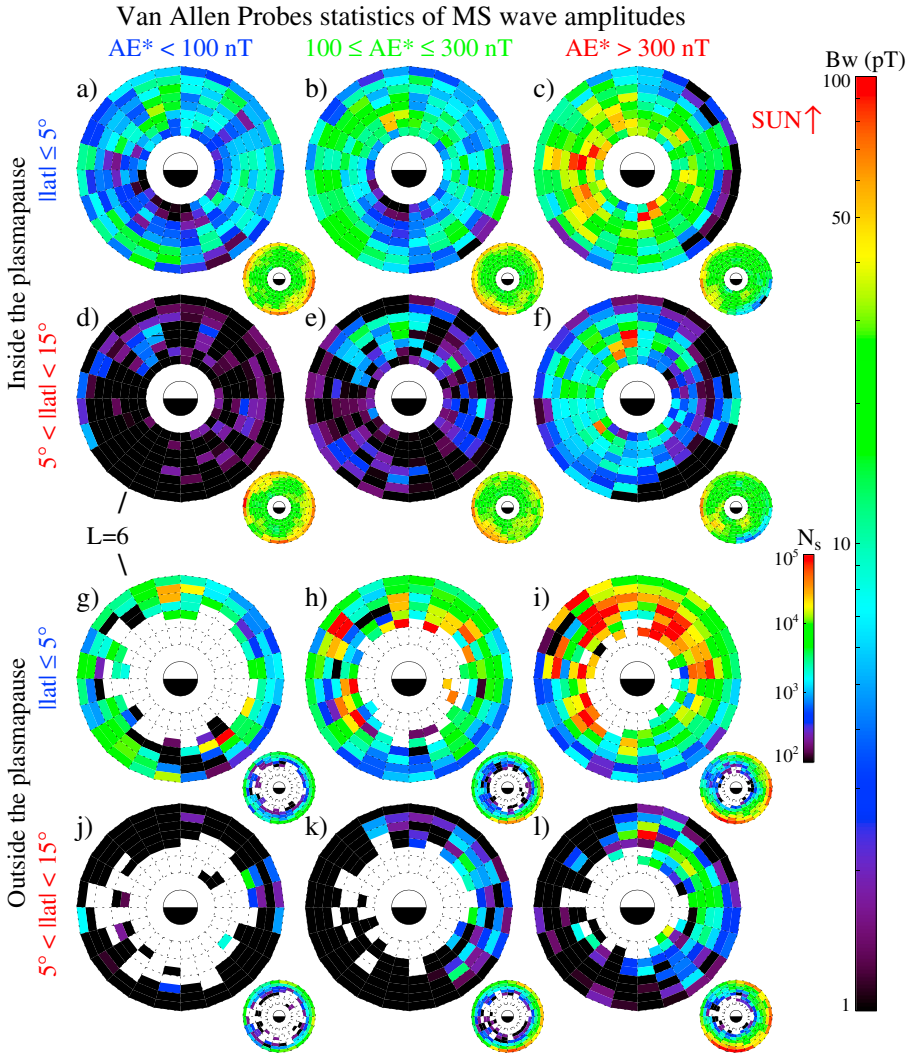

Figure 2. The global distribution of RMS wave amplitude B_w for $2 < L < 6$. The wave intensity is categorized by magnetic latitude and *AE** and shown for locations (a–f) inside and (g–l) outside the plasmapause. The sample number (N_s) is shown in smaller plots at the right bottom corner of each panel. White area represents the region where N_s is less than 100.

obtained between 2001 and 2010 [*Mourenas et al.*, 2013; *Němec et al.*, 2015]. Both the Van Allen Probes survey and the previous statistics show that the strongest magnetosonic waves are observed between 3 R_E and 5 R_E, on the dayside, outside the plasmapause, near the equator, and during disturbed conditions. During quiet geomagnetic periods, the peak wave amplitude is around 40 pT near the dayside and outside the plasmapause, which is consistent with the Cluster statistical result by *Mourenas et al.* [2013]. When *AE** is higher than 300 nT, the RMS averaged wave amplitude outside the plasmapause is between 50 and 100 pT on the dayside and around 20 pT on the nightside, and the RMS averaged wave amplitude inside the plasmapause peaks around 50 pT near the duskside and is mostly around 20 pT in other MLT sectors. The recent Cluster statistics by *Němec et al.* [2015] have shown similar features in their variation with geomagnetic activity and the wave MLT distributions both inside and outside the plasmapause. The Van Allen Probes provide extensive spatial data coverage at $L < 6$ especially near the equator or inside the plasmapause, where previous satellite data coverage was limited [e.g., *Meredith et al.*, 2008; *Ma et al.*, 2013]. We also note that a broader range of geomagnetic conditions was sampled by the Van Allen probes. For instance, more intense magnetosonic wave events are observed by the Van Allen Probes especially when *AE** > 300 nT than the previous THEMIS survey [*Ma et al.*, 2013] which was obtained during a relatively quiet period.

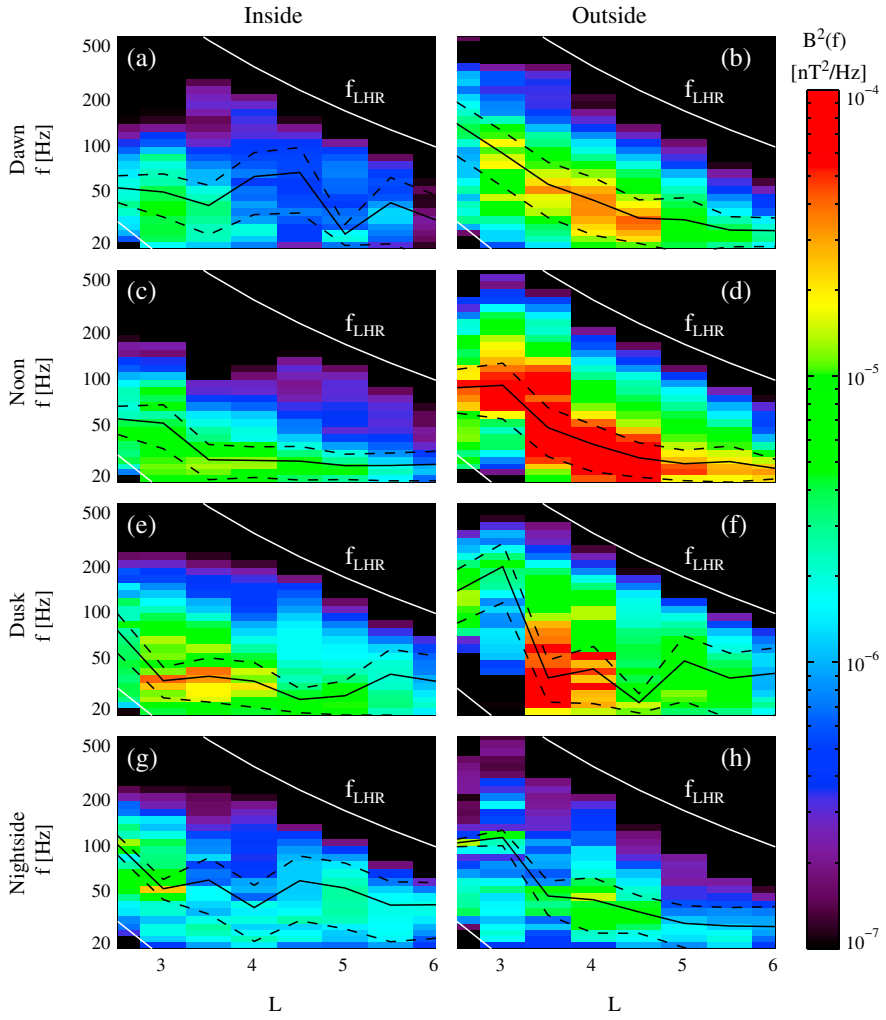

Figure 3. The survey of magnetosonic wave magnetic field power intensity inside and outside the plasmapause, as a function of wave frequency and *L* shell. The wave spectra are categorized into different MLT sectors: Dawn (3–9 MLT), Noon (9–15 MLT), Dusk (15–21 MLT), and Nightside (21–3 MLT). The two white solid lines represent the frequencies of f_{LHR} (above) and f_{cp} (below) respectively; the black solid line represents the frequency with peak wave intensity; and the two black dashed lines represent the standard derivations.

We use the WFR data from the Van Allen Probes statistics to obtain the statistical magnetosonic wave frequency spectra. Figure 3 presents a survey of the time-averaged magnetosonic wave intensity distribution as a function of *L* shell and wave frequency, categorized by whether it is observed inside or outside the plasmapause and further divided into different magnetic local time (MLT) sectors with an MLT width of 6 h. The white solid lines in each panel denote the lines of f_{LHR} (above) and f_{cp} (below), which are estimated from a dipole magnetic field. Consistent with the global survey of wave amplitude distributions, the most intense magnetosonic waves are located near the noon sector, between 3 R_E and 5 R_E, outside the plasmapause, with a peak wave frequency (the black solid line) between 30 Hz and 100 Hz. The wave frequency from the statistical survey follows the variation of f_{LHR} and f_{cp} outside the plasmapause, while this trend is not clear inside the plasmapause. This feature is consistent with the frequency features of the observed individual wave events and explained as a combined effect of wave local excitation and perpendicular propagation [e.g., *Ma et al*., 2014a, 2014b]. We normalize the wave intensity spectra and perform a Gaussian fitting of the wave frequency spectra at different locations to obtain the wave frequency information and combine the results with the wave amplitude distributions in Figure 2 to calculate the general scattering rates due to magnetosonic waves.

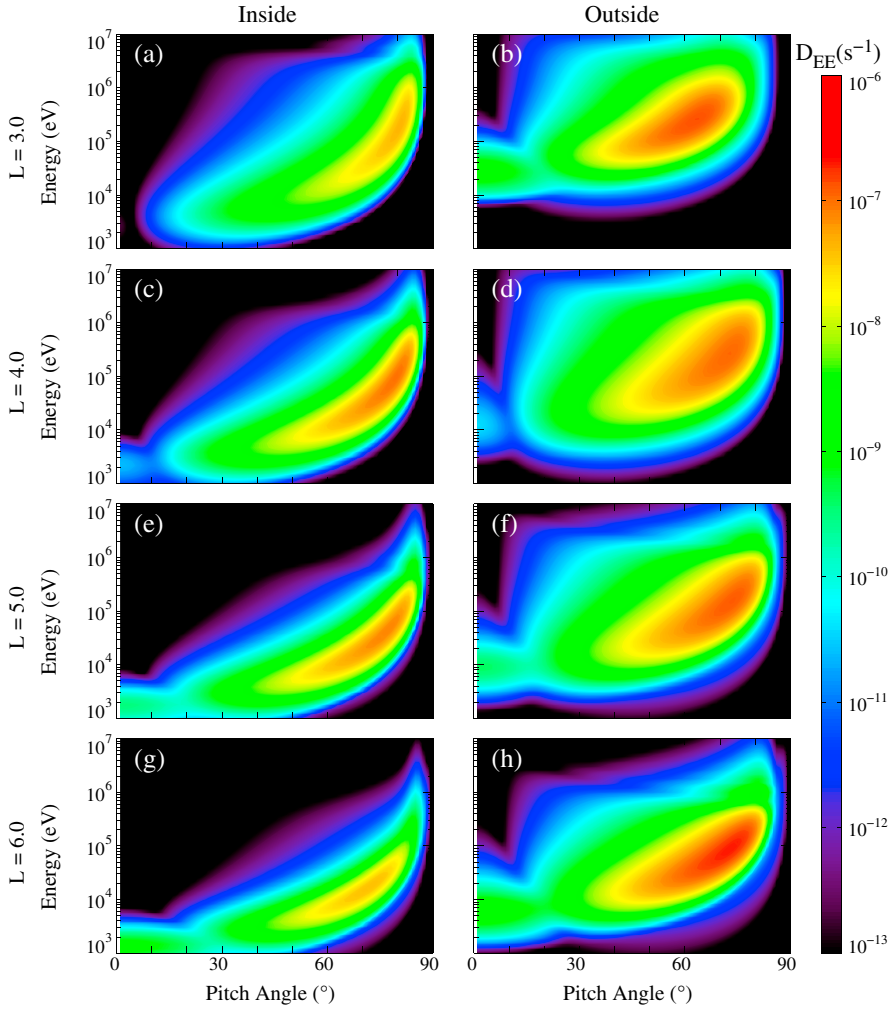

Figure 4. The drift and bounce averaged energy diffusion coefficients due to magnetosonic waves as a function of pitch angle and energy during disturbed conditions ($AE^* > 300$ nT) inside and outside the plasmapause from $L = 3$ to $L = 6$.

3. Electron Scattering Due to Statistical Magnetosonic Waves

The magnetosonic waves are spatially localized near the geomagnetic equator within ~ 2°–3° in latitude consistent with previous observations [e.g., *Němec et al.*, 2005, 2006; *Pokhotelov et al.*, 2008; *Santolík et al.*, 2004]. *Bortnik et al.* [2015] have simplified the motions of electrons streaming through the magnetosonic waves using several reasonable assumptions: (1) the wave magnetic field B_w is confined to regions near the geomagnetic equator, with a latitudinal scale width λ_w and described by a Gaussian distribution $B_w = B_{w,0} \exp(-\lambda^2/\lambda_w^2)$; (2) higher harmonic resonances with harmonic number $|N| \geq 1$ are ignored, because generally the first-order cyclotron resonance requires a resonance energy higher than ~ 10 MeV; and (3) adiabatic variations of the particle's motion are ignored because the interactions occur only in the vicinity of the magnetic equator, which requires that the initial pitch angle of the electrons should be less than ~80°. The analytical formula includes both Landau resonance and transient-time scattering effects and is an accurate estimate for the full test-particle calculations [*Bortnik et al.*, 2015]. Full test-particle calculation and the analytical formula are consistent with the quasi-linear theory calculations near the Landau resonance regime, and they also evaluate the scattering rates at pitch angles and energies away from the Landau resonance regime which are dominated by the transit-time effects and would be absent in the quasi-linear paradigm [*Li et al.*, 2014a]. The calculation of the diffusion coefficients using the analytical formula has been proven to be both computationally efficient and accurate in capturing the important scattering features of equatorial magnetosonic waves.

We use the analytical formula [*Bortnik et al*., 2015] and the Van Allen Probes statistics to evaluate the general scattering effects of magnetosonic waves at different locations and under different conditions. The wave normal angle (ψ) distribution is assumed to be Gaussian in $X = \tan\psi$ with a peak at 89° and a width $X_w = \tan 86°$, following *Horne et al*. [2007]. Consistent with *Bortnik et al*. [2015], the wave latitudinal scale width is assumed to be 2° from the equator. The background magnetic field is approximated as a dipole magnetic field, and we use Sheeley's density models in the plasmasphere and the plasmatrough [*Sheeley et al*., 2001] to estimate the total electron densities. The diffusion coefficients are then averaged over the bounce period and along the drift path over different MLT sectors.

Figure 4 presents the energy diffusion coefficients at different *L* shells calculated under disturbed conditions (when $AE^* > 300$ nT) both inside and outside the plasmapause. Previous studies have found that the magnetosonic waves mainly cause electron acceleration, and the energy diffusion coefficients can be used to estimate the timescale of electron energization. The peak profile of the diffusion coefficient indicates the trend of Landau resonance, and the transit-time effect causes the additional scattering over a much broader pitch angle and energy range.

The energization of electrons due to magnetosonic waves is most efficient outside the plasmapause during disturbed conditions. Inside the plasmapause, the RMS averaged wave amplitudes are weaker, and the scattering occurs over a much narrower pitch angle range than outside the plasmapause. In general, as *L* shell increases, the ratio of plasma frequency to the electron gyrofrequency (f_{pe}/f_{ce}) increases, the magnetosonic waves cause electron scattering at higher (and over narrower) pitch angle ranges and lower energy ranges. Electrons over the pitch angle range of 50° to 80° and energy range of 10 keV to several MeV may be accelerated via Landau resonance. The highest-energy diffusion coefficient corresponds to an acceleration timescale of more than 10 days, which is considerably slower than the electron energization by whistler-mode chorus waves under similar conditions on a timescale of several hours to ~1 day [e.g., *Summers et al*., 2002; *Horne et al*., 2005; *Thorne et al*., 2013]. Similarly, *Mourenas et al*. [2013] have shown that the energy diffusion by magnetosonic waves is generally weaker than diffusion by chorus waves during quiet geomagnetic periods. The electron scattering by magnetosonic waves is sensitive to the wave normal angle distribution as shown by *Mourenas et al*. [2013]. However, the magnetosonic wave normal is highly oblique, and the exact wave normal angle distribution is not accurately known yet from satellite observations or ray tracing models.

Figure 5 shows the simulation of electron scattering due to magnetosonic waves at $L = 4$ during disturbed conditions ($AE^* > 300$ nT). The drift and bounce averaged pitch angle, momentum, and mixed pitch angle-momentum diffusion coefficients ($D\alpha\alpha$, Dpp, and $D\alpha p$) are shown in Figures 5a–5c. The RMS statistical wave amplitudes are ~ 60 pT on the dayside and ~ 25 pT on the nightside, and the wave peak frequency is ~ 40 Hz. Because Landau resonance causes electron acceleration along the $v_{||}$ direction, an increase in electron energy corresponds to a decrease in electron pitch angle, and $D\alpha p$ is mainly negative. Because the adiabatic variation of the particle is ignored within 2° near the equator, the electron pitch angle should be less than 83.3° (the white dashed lines in Figures 5a–5c) for a maximum error of 20% in the rate of phase angle accumulation [e.g., see *Bortnik et al*., 2015, equation (20)]. The pitch angle diffusion coefficients are less than $10^{-9}\,s^{-1}$ (timescale of >30 years) at pitch angles less than ~ 25° at different energies. Therefore, the magnetosonic waves do not cause significant electron precipitation into the Earth's upper atmosphere.

We simulate the evolution of electron phase space density *f* by numerically solving the 2-D Fokker-Planck equation using the Alternative Directional Implicit method [*Xiao et al*., 2009]. The lower and higher-energy boundary conditions are set as constant at energies of 10 keV and 10 MeV, respectively. $f(\alpha \le \alpha_{LC}) = 0$ is assumed at different energies to simulate an empty loss cone, where α is the electron pitch angle and α_{LC} is the bounce loss cone. At the higher-pitch angle boundary, we assume that $\frac{\partial f}{\partial \alpha}|_{\alpha=90^\circ} = 0$. For simplicity, the initial PSD distribution of the electrons is modeled using a kappa distribution with the kappa index $\kappa = 6$ following the study by *Xiao et al*. [2008]:

$$f(\alpha, p) = \left(1 + \frac{p^2}{\kappa\theta^2}\right)^{-(k+1)} \sin\alpha, \tag{1}$$

where *p* is the electron momentum normalized by $m_e c$, m_e is the electron mass, *c* is the light speed, and θ is the effective thermal parameter scaled by the electron rest mass and is set as $\theta^2 = 0.15$. The PSD values are normalized and do not contain units.

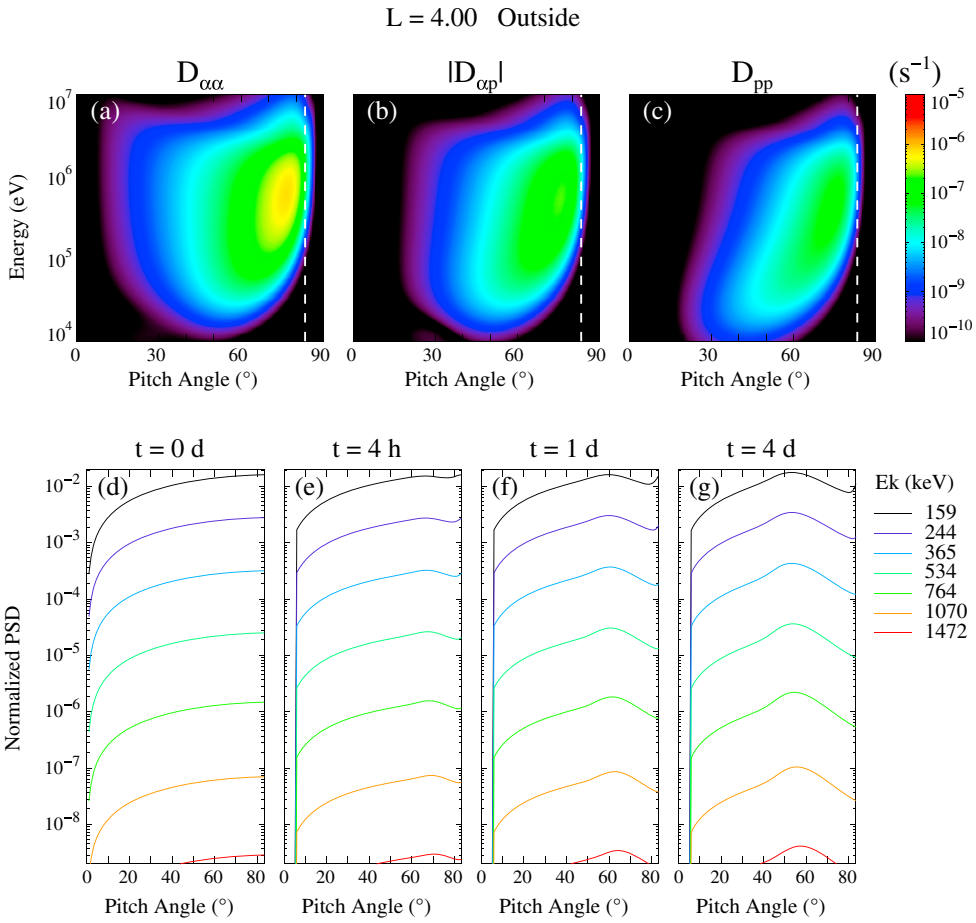

Figure 5. The simulation of electron scattering due to magnetosonic waves at $L = 4$ outside the plasmapause during disturbed conditions. (a–c) The drift and bounce averaged pitch angle, absolute values of mixed pitch angle-momentum, and momentum diffusion coefficients as a function of pitch angle and energy. The majority of the mixed pitch angle-momentum diffusion coefficients are negative. The white dashed line indicates a pitch angle of 83.3°. At pitch angles larger than 83.3°, the errors in the rate of phase angle accumulation are larger than 20%. (d–g) The simulated evolution of electron pitch angle distributions at selected energies for a period of 4 days. The pitch angle range is from 0° to 83.3°. The initial electron PSD distributions are normalized and assumed to follow a Kappa distribution with $\kappa = 6$.

Figures 5d–5g present the results of a 4 day simulation of the electron pitch angle distribution from ~150 keV to ~1.5 MeV. The scattering effects of magnetosonic waves are small over a timescale of several hours. However, after 1 day, the electron PSD at pitch angles between 50° and 70° increases and the PSD at higher pitch angles decreases, forming a noticeable butterfly distribution at energies of hundreds of keV. The simulation demonstrates that intense magnetosonic waves may be an important factor for the formation of the observed butterfly distribution of energetic electrons in the absence of other scattering waves. A careful examination on the electron evolution shows that the electron PSD increase occurs earlier at higher pitch angles, and the particles are subsequently scattered from higher pitch angles and lower energies toward lower pitch angles and higher energies. The PSD evolution property is consistent with the scenario of electron acceleration by Landau resonance, which mainly increases the parallel velocity of the electron in its moving frame.

We perform a similar simulation of the electron evolution at $L = 3.5$ inside the plasmapause as shown in Figure 6. The wave amplitude is ~ 50 pT on the duskside and ~ 20 pT for other MLT sectors, and the wave peak frequency is ~ 40 Hz. The diffusion coefficients ($D\alpha\alpha$, Dpp, and $D\alpha p$) in Figures 6a–6c demonstrate that the electron scattering rates are limited within narrower and higher-pitch angle ranges, although the peak diffusion rates are higher than the scattering outside the plasmapause. The major energy band of effective Landau resonance is slightly lower than the energy band outside the plasmapause and is also within the energy range of 10 keV–1 MeV. The

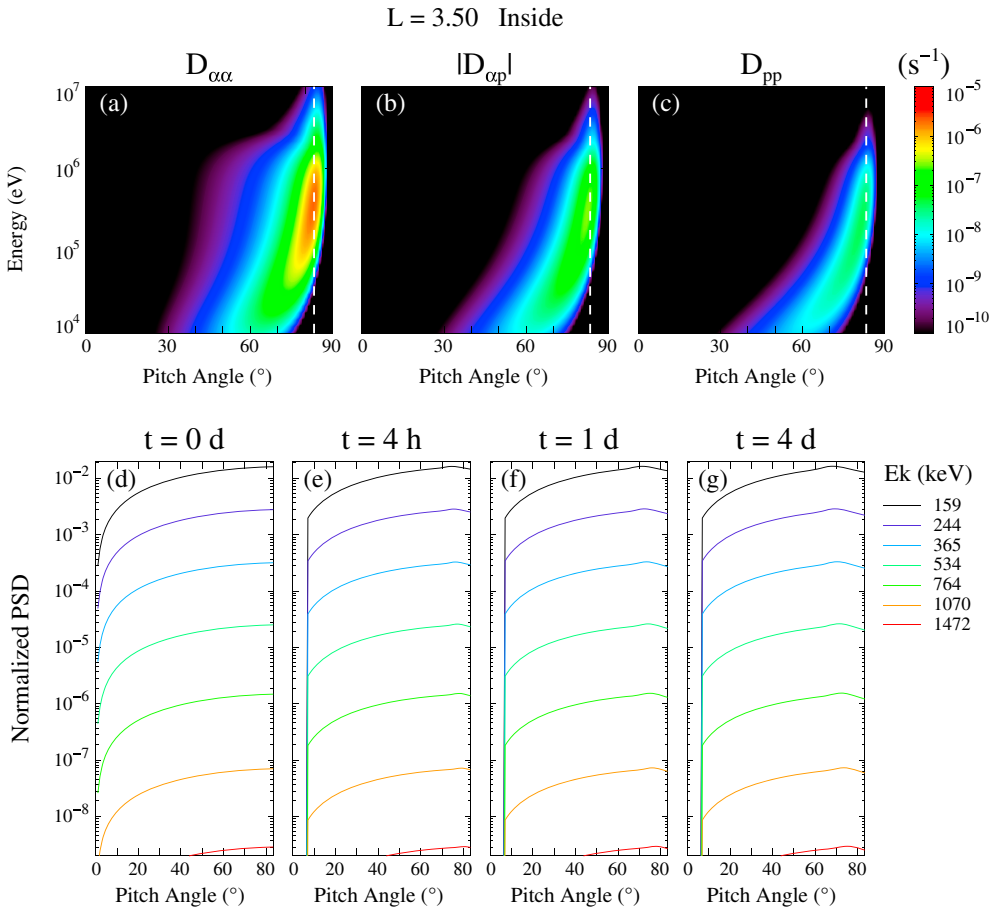

Figure 6. The same format as Figure 5 except for $L = 3.5$ inside the plasmapause.

pitch angle scattering rates become extremely weak at pitch angles below ~ 30°, indicating that magnetosonic waves do not cause precipitation loss of energetic electrons inside the plasmasphere. However, the presence of other wave modes (e.g., plasmaspheric hiss) can reduce the lifetime of energetic electrons and cause more efficient electron precipitation losses [e.g., *Meredith et al.*, 2009; *Mourenas et al.,* 2013].

Figures 6d–6g present the electron PSD distribution evolution in the same format as Figures 5d–5g. Compared with the results outside the plasmapause, the electrons are only slightly scattered over a timescale of 4 days, and the electron PSD at ~ 70° increases slightly after 4 days. This suggests that these statistically averaged magnetosonic waves cannot effectively energize electrons inside the plasmasphere on the timescale of ~1 day. However, extremely strong magnetosonic waves with wave amplitudes of ~1 nT may occasionally lead to the rapid formation of butterfly distribution of electrons [*Xiao et al.,* 2015].

4. Conclusions and Discussions

Using the Van Allen Probes wave statistics and the analytical formula for the diffusion coefficients, we have analyzed the typical electron scattering rates due to magnetosonic waves under different conditions in the Earth's inner magnetosphere. The global distributions of magnetosonic wave amplitudes and frequency spectra have been obtained from a recent 31 month period of Van Allen Probes wave data. Analytical formulae for electron scattering [*Bortnik et al.,* 2015] have been employed to provide an efficient and numerically accurate means to evaluate the scattering rates due to Landau resonance and transit-time effects of magnetosonic waves. The diffusion coefficients of magnetosonic waves at different locations and under different conditions are calculated, and simulations of the electron PSD evolution during the interactions with magnetosonic waves are performed outside and inside the plasmapause separately.

Our principal results are summarized as follows.1. The global distribution of magnetosonic waves based on the Van Allen Probes survey generally shows similar characteristics to previous studies but with stronger wave intensities particularly during active geomagnetic conditions ($AE^* > 300$ nT).2. The wave frequency spectrum statistics present different properties outside and inside the plasmapause, and the wave frequency spectra more closely follow the radial variation of f_{LHR} outside the plasmapause than inside.3. During disturbed conditions, the magnetosonic waves outside the plasmasphere can cause significant electron acceleration from ~100 keV to a few MeV over a timescale of several days.4. The RMS averaged magnetosonic waves may be responsible for forming butterfly distributions of the energetic electrons outside the plasmapause over a timescale of several days.5. The electrons are mainly accelerated via Landau resonance, therefore, the lower energy and higher-pitch angle electron populations are scattered into a regime with higher energy and lower pitch angle.6. In general, the electron acceleration due to magnetosonic wave is less efficient than the electron heating by whistler-mode chorus wave events.

Our simulations show that the intense magnetosonic waves may potentially account for the formation of butterfly distributions of hundreds keV electrons, which are occasionally observed in the inner magnetosphere [*Zhao et al.,* 2014; *Artemyev et al.,* 2015]. Although magnetopause shadowing and nightside magnetic field deformation [*Artemyev et al.,* 2015] can lead to the formation of electron butterfly distributions particularly at larger *L* shells (> ~5), our study and the simulation by *Xiao et al.* [2015] indicate that the electron scattering by magnetosonic waves is an important mechanism for producing butterfly distributions at relatively lower *L* shells especially in the regions with intense magnetosonic wave activities. Extremely strong magnetosonic wave events with amplitudes of several nanoteslas have occasionally been detected [e.g., *Zhou et al.,* 2014]. These extremely strong magnetosonic waves are expected to efficiently cause the electron acceleration and form the butterfly distribution over a short timescale of several minutes to hours [*Xiao et al.,* 2015]. The magnetosonic waves can also scatter the electrons with high pitch angles near 90° by bounce resonance interactions [*Shprits,* 2009; *Chen et al.,* 2015]. The electron diffusion coefficients due to magnetosonic waves are sensitive to various parameters (e.g., total plasma density and wave normal angle), and the pitch angle ranges of the resultant butterfly distributions are related to the event-specific background plasma condition and the wave properties. It is also worth noting that the diffusion coefficients at pitch angles between ~80° and 90° may not be well represented by the analytical formula due to the assumptions; therefore, the lack of magnetosonic wave scattering near 90° in our simulations may not be completely accurate. Full test-particle simulations could incorporate the bounce resonance effects [*Chen et al.,* 2015], but this is beyond the scope of our study. Nevertheless, our study provides essential information on the relative role of statistically averaged magnetosonic waves in the Earth's radiation belts under typical geomagnetic conditions.

Acknowledgments

The authors would like to gratefully acknowledge the support of NSF's Geospace Environment Modeling grant AGS-1103064, NSF/DOE basic plasma physics partnership program, grant DE-SC0010578, and NASA grants NNX11AR64G, NNX14AI18G, and by JHU/APL contracts 967399 and 921647 under NASA's prime contract NAS5-01072, AFOSR grant FA9550-15-1-0158, and NSF grants AGS 1405041 and 1405054. The analysis at UCLA was supported by the EMFISIS subaward 1001057397:01. In this paper, the EMFISIS data are available from http://emfisis.physics.uiowa.edu/Flight/. We thank the World Data Center for Geomagnetism, Kyoto, for providing *AE* indices used in this study.

References

Artemyev, A. V., O. V. Agapitov, F. S. Mozer, and H. Spence (2015), Butterfly pitch angle distribution of relativistic electrons in the outer radiation belt: Evidence of nonadiabatic scattering, *J. Geophys. Res. Space Physics*, *120*, 4279–4297, doi:10.1002/2014JA020865.

Boardsen, S. A., D. L. Gallagher, D. A. Gurnett, W. K. Peterson, and J. L. Green (1992), Funnel-shaped, low-frequency equatorial waves, *J. Geophys. Res.*, *97*(A10), 14,967–14,976, doi:10.1029/92JA00827.

Bortnik, J., and R. M. Thorne (2010), Transit time scattering of energetic electrons due to equatorially confined magnetosonic waves, *J. Geophys. Res.*, *115*, A07213, doi:10.1029/2010JA015283.

Bortnik, J., R. M. Thorne, B. Ni, and J. Li (2015), Analytical approximation of transit time scattering due to magnetosonic waves, *Geophys. Res. Lett.*, *42*, 1318–1325, doi:10.1002/2014GL062710.

Chen, L., and R. M. Thorne (2012), Perpendicular propagation of magnetosonic waves, *Geophys. Res. Lett.*, *39*, L14102, doi:10.1029/2012GL052485.

Chen, L., R. M. Thorne, V. K. Jordanova, and R. B. Horne (2010), Global simulation of magnetosonic wave instability in the storm time magnetosphere, *J. Geophys. Res.*, *115*, A11222, doi:10.1029/2010JA015707.

Chen, L., R. M. Thorne, V. K. Jordanova, M. F. Thomsen, and R. B. Horne (2011), Magnetosonic wave instability analysis for proton ring distributions observed by the LANL magnetospheric plasma analyzer, *J. Geophys. Res.*, *116*, A03223, doi:10.1029/2010JA016068.

Chen, L., A. Maldonado, J. Bortnik, R. M. Thorne, J. Li, L. Dai, and X. Zhan (2015), Nonlinear bounce resonances between magnetosonic waves and equatorially mirroring electrons, *J. Geophys. Res. Space Physics*, *120*, 6514–6527, doi:10.1002/2015JA021174.

Foster, J. C., et al. (2014), Prompt energization of relativistic and highly relativistic electrons during a substorm interval: Van Allen Probes observations, *Geophys. Res. Lett.*, *41*, 20–25, doi:10.1002/2013GL058438.

Horne, R. B., R. M. Thorne, S. A. Glauert, J. M. Albert, N. P. Meredith, and R. R. Anderson (2005), Timescale for radiation belt electron acceleration by whistler mode chorus waves, *J. Geophys. Res.*, *110*, A03225, doi:10.1029/2004JA010811.

Horne, R. B., R. M. Thorne, S. A. Glauert, N. P. Meredith, D. Pokhotelov, and O. Santolik (2007), Electron acceleration in the Van Allen radiation belts by fast magnetosonic waves, *Geophy. Res. Lett.*, *34*, S09S03, doi:10.1029/L17107.

Jordanova, V. K., D. T. Welling, S. G. Zaharia, L. Chen, and R. M. Thorne (2012), Modeling ring current ion and electron dynamics and plasma instabilities during a high speed stream driven storm, *J. Geophys. Res.*, *117*, A00L08, doi:10.1029/2011JA017433.

Kasahara, Y., H. Kenmochi, and I. Kimura (1994), Propagation characteristics of the ELF emissions observed by the satellite Akebono in the magnetic equatorial region, *Radio Sci.*, *29*(4), 751–767, doi:10.1029/94RS00445.

Kennel, C. F., and F. Engelmann (1966), Velocity space diffusion from weak plasma turbulence in a magnetic field, *Phys. Fluids*, *9*, 2377–2388, doi:10.1063/1.1761629.

Kletzing, C., et al. (2013), The electric and magnetic field instrument suite and integrated science (EMFISIS) on RBSP, *Space Sci. Rev.*, *179*(1–4), 127–181, doi:10.1007/s11214-013-9993-6.

Kurth, W. S., S. De Pascuale, J. B. Faden, C. A. Kletzing, G. B. Hospodarsky, S. Thaller, and J. R. Wygant (2015), Electron densities inferred from plasma wave spectra obtained by the Waves instrument on Van Allen Probes, *J. Geophys. Res. Space Physics*, *120*, 904–914, doi:10.1002/2014JA020857.

Laakso, H., H. Junginger, A. Roux, R. Schmidt, and C. de Villedary (1990), Magnetosonic waves above $f_c(H^+)$ at geostationary orbits: GEOS 2 results, *J. Geophys. Res.*, *95*(A7), 10,609–10,621, doi:10.1029/JA095iA07p10609.

Li, J., et al (2014a), Interactions between magnetosonic waves and radiation belt electrons: Comparisons of quasi-linear calculations with test particle simulations, *Geophys. Res. Lett.*, *41*, 4828–4834, doi:10.1002/2014GL060461.

Li, W., et al. (2014b), Radiation belt electron acceleration by chorus waves during the 17 March 2013 storm, *J. Geophys. Res. Space Physics*, *119*, 4681–4693, doi:10.1002/2014JA019945.

Lyons, L. R. (1974a), General relations for resonant particle diffusion in pitch angle and energy, *J. Plasma Phys.*, *12*, 45–49, doi:10.1017/S0022377800024910.

Lyons, L. R. (1974b), Pitch angle and energy diffusion coefficients from resonant interactions with ion cyclotron and whistler waves, *J. Plasma Phys.*, *12*, 417–432, doi:10.1017/S002237780002537X.

Ma, Q., W. Li, R. M. Thorne, and V. Angelopoulos (2013), Global distribution of equatorial magnetosonic waves observed by THEMIS, *Geophys. Res. Lett.*, *40*, 1895–1901, doi:10.1002/grl.50434.

Ma, Q., W. Li, L. Chen, R. M. Thorne, and V. Angelopoulos (2014a), Magnetosonic wave excitation by ion ring distribution in the Earth's inner magnetosphere, *J. Geophys. Res. Space Physics*, *119*, 844–852, doi:10.1002/2013JA019591.

Ma, Q., W. Li, L. Chen, R. M. Thorne, C. A. Kletzing, W. S. Kurth, G. B. Hospodarsky, G. D. Reeves, M. G. Henderson, and H. E. Spence (2014b), The trapping of equatorial magnetosonic waves in the Earth's outer plasmasphere, *Geophys. Res. Lett.*, *41*, 6307–6313, doi:10.1002/2014GL061414.

Mauk, B. H., N. J. Fox, S. G. Kanekal, R. L. Kessel, D. G. Sibeck, and A. Ukhorskiy (2012), Science objectives and rationale for the Radiation Belt Storm Probes mission, *Space Sci. Rev.*, *1–15*, doi:10.1007/s11214-012-9908-y.

Meredith, N. P., R. B. Horne, R. M. Thorne, D. Summers, and R. R. Anderson (2004), Substorm dependence of plasmaspheric hiss, *J. Geophys. Res.*, *109*, A06209, doi:10.1029/2004JA010387.

Meredith, N. P., R. B. Horne, S. A. Glauert, D. N. Baker, S. G. Kanekal, and J. M. Albert (2009), Relativistic electron loss timescales in the slot region, *J. Geophys. Res.*, *114*, A03222, doi:10.1029/2008JA013889.

Meredith, N., R. B. Horne, and R. R. Anderson (2008), Survey of magnetosonic waves and proton ring distributions in the Earth's inner magnetosphere, *J. Geophys. Res.*, *113*, A06213, doi:10.1029/2007JA012975.

Mourenas, D., A. V. Artemyev, O. V. Agapitov, and V. Krasnoselskikh (2013), Analytical estimates of electron quasi-linear diffusion by fast magnetosonic waves, *J. Geophys. Res. Space Physics*, *118*, 3096–3112, doi:10.1002/jgra.50349.

Němec, F., O. Santolík, K. Gereová, E. Macúšová, Y. de Conchy, and N. Cornilleau-Wehrlin (2005), Initial results of a survey of equatorial noise emissions observed by the Cluster spacecraft, *Planet. Space Sci.*, *53*(1–3), 291–298, doi:10.1016/j.pss.2004.09.055.

Němec, F., O. Santolík, K. Gereová, E. Macúšová, H. Laakso, Y. de Conchy, M. Maksimovic, and N. Cornilleau-Wehrlin (2006), Equatorial noise: Statistical study of its localization and the derived number density, *Adv. Space Res.*, *37*(3), 610–616, doi:10.1016/j.asr.2005.03.025.

Němec, F., O. Santolík, Z. Hrbáčková, and N. Cornilleau-Wehrlin (2015), Intensities and spatiotemporal variability of equatorial noise emissions observed by the Cluster spacecraft, *J. Geophys. Res. Space Physics*, *120*, 1620–1632, doi:10.1002/2014JA020814.

Perraut, S., A. Roux, P. Robert, and R. Gendrin (1982), A systematic study of ULF waves above FH+ from GEOS 1 and 2 measurements and their relationships with proton ring distributions, *J. Geophys. Res.*, *87*(A8), 6219–6236, doi:10.1029/JA087iA08p06219.

Pokhotelov, D., F. Lefeuvre, R. B. Horne, and N. Cornilleau-Wehrlin (2008), Survey of ELF-VLF plasma waves in outer radiation belt observed by Cluster staff experiment, *Ann. Geophys.*, *26*(11), 3269–3277, doi:10.5194/angeo-26-3269-2008.

Reeves, G. D., et al. (2013), Electron acceleration in the heart of the Van Allen radiation belts, *Science*, *341*, 991–994, doi:10.1126/science.1237743.

Russell, C. T., and R. E. Holzer (1970), OGO 3 observation of ELF noise in the magnetosphere 2. The nature of the Equatorial noise, *J. Geophys. Res.*, *75*(4), 755–768, doi:10.1029/JA075i004p00755.

Santolík, O., J. S. Pickett, and D. A. Gurnett (2002), Spatiotemporal variability and propagation of equatorial noise observed by Cluster, *J. Geophys. Res.*, *107*(A12), 1495, doi:10.1029/2001JA009159.

Santolík, O., M. Parrot, and F. Lefeuvre (2003), Singular value decomposition methods for wave propagation analysis, *Radio Sci.*, *38*, 1010, doi:10.1029/2000RS002523.

Santolík, O., F. Němec, K. Gereová, E. Macúšová, Y. de Conchy, and N. Cornilleau-Wehrlin (2004), Systematic analysis of equatorial noise below the lower hybrid frequency, *Ann. Geophys.*, *22*, 2587–2595, doi:10.5194/angeo-22-2587-2004.

Sheeley, B. W., M. B. Moldwin, H. K. Rassoul, and R. R. Anderson (2001), An empirical plasmasphere and trough density model: CRRES observations, *J. Geophys. Res.*, *106*(A11), 25,631–25,641, doi:10.1029/2000JA000286.

Shprits, Y. Y. (2009), Potential waves for pitch-angle scattering of near-equatorially mirroring energetic electrons due to the violation of the second adiabatic invariant, *Geophys. Res. Lett.*, *36*, L12106, doi:10.1029/2009GL038322.

Summers, D., C. Ma, N. P. Meredith, R. B. Horne, R. M. Thorne, D. Heynderickx, and R. R. Anderson, (2002) Model of the energization of outer-zone electrons by whistler-mode chorus during the October 9, 1990 geomagnetic storm, *Geophys. Res. Lett.*, *29*(24), 2174, doi:10.1029/2002GL016039.

Thomsen, M. F., M. H. Denton, V. K. Jordanova, L. Chen, and R. M. Thorne (2011), Free energy to drive equatorial magnetosonic wave instability at geosynchronous orbit, *J. Geophys. Res.*, *116*, A08220, doi:10.1029/2011JA016644.

Thorne, R. M. (2010), Radiation belt dynamics: The importance of wave-particle interactions, *Geophys. Res. Lett.*, *37*, L22107, doi:10.1029/2010GL044990.

Thorne, R. M., et al. (2013), Rapid local acceleration of relativistic radiation-belt electrons by magnetospheric chorus, *Nature*, *504*, 411–414, doi:10.1038/nature12889.

Xiao, F., C. Shen, Y. Wang, H. Zheng, and S. Wang (2008), Energetic electron distributions fitted with a relativistic kappa-type function at geosynchronous orbit, *J. Geophys. Res.*, *113*, A05203, doi:10.1029/2007JA012903.

Xiao, F., Z. Su, H. Zheng, and S. Wang (2009), Modeling of outer radiation belt electrons by multidimensional diffusion process, *J. Geophys. Res.*, *114*, A03201, doi:10.1029/2008JA013580.

Xiao, F., Q. Zhou, Z. He, and L. Tang (2012), Three-dimensional ray tracing of fast magnetosonic waves, *J. Geophys. Res.*, *117*, A06208, doi:10.1029/2012JA017589.

Xiao, F., Q. Zhou, Z. He, C. Yang, Y. He, and L. Tang (2013), Magnetosonic wave instability by proton ring distributions: Simultaneous data and modeling, *J. Geophys. Res. Space Physics*, *118*, 4053–4058, doi:10.1002/jgra.50401.

Xiao, F., C. Yang, Z. Su, Q. Zhou, Z. He, Y. He, D. N. Baker, H. E. Spence, H. O. Fusten, and J. B. Blake (2015), Wave-driven butterfly distribution of Van Allen belt relativistic electrons, *Nat. Commun.*, *6*, 8590, doi:10.1038/ncomms9590.

Zhao, H., X. Li, J. B. Blake, J. F. Fennell, S. G. Claudepierre, D. N. Baker, A. N. Jaynes, and D. M. Malaspina (2014), Characteristics of pitch angle distributions of hundreds of keV electrons in the slot region and inner radiation belt, *J. Geophys. Res. Space Physics*, *119*, 9543–9557, doi:10.1002/2014JA020386.

Zhou, M., B. Ni, S. Huang, X. Deng, M. Ashour-Abdalla, Y. Nishimura, Z. Yuan, Y. Pang, and H. Li (2014), Observation of large-amplitude magnetosonic waves at dipolarization fronts, *J. Geophys. Res. Space Physics*, *119*, 4335–4347, doi:10.1002/2014JA019796.